

Diffusing-Wave Spectroscopy: The Technique and Some Applications

D. A. Weitz,¹ J. X. Zhu,² D. J. Durian,³ Hu Gang¹ and D. J. Pine¹

¹ Exxon Research and Engineering Co., Rt. 22E, Annandale, NJ 08801 U.S.A.

² Dept. of Chemical Engineering, Princeton University, Princeton, NJ 08540 U.S.A.

³ Dept. of Physics, University of California at Los Angeles, Los Angeles, CA 90024 U.S.A.

Received March 29, 1993; accepted April 18, 1993

Abstract

We discuss the extension of dynamic light scattering to very strongly scattering media, where the propagation of light is described by the diffusion approximation, allowing the distribution of the light paths to be determined. The temporal evolution of the length of each of these paths, due to the dynamics of the scattering medium, is calculated, and an expression for the temporal autocorrelation function of the intensity fluctuations of the scattered light is obtained. This relates the measured decay of the autocorrelation function to the dynamics of the medium. This technique is called diffusing wave spectroscopy (DWS). To extend its utility, we consider the consequences of interactions between the scattering particles on the light scattering. To illustrate its applications, we consider several examples of new physics that can be investigated using DWS. We study the transient nature of hydrodynamic interactions between a particle and the surrounding fluid. We are able to probe the decay of the velocity correlation function of the particles, and we demonstrate its algebraic decay, with a $t^{-3/2}$ time dependence. We also show that the time-dependent self diffusion coefficient exhibits an unexpected scaling behavior, whereby all the data, from samples of different volume fractions, can be scaled onto a single curve. Finally, we discuss the applications of DWS to the study of the dynamics of foams, and show how it can be used to probe the rearrangement of the bubbles within the foam as they coarsen.

1. Introduction

The propagation of waves through very strongly scattering media is a subject of intense and widespread interest. Initially, much of the work focused on the behavior of electrons, and the effort was driven by the quest for localization of the electrons due to strong scattering. More recently, additional effort has focused on classical waves, with the recognition that light should exhibit many of the same effects as electrons when it propagates through a medium that strongly scatters it. Important early results demonstrated the close analogy between light and electrons by observing the behavior of the backscattered light from a very strongly scattering medium [1, 2]. It exhibits a narrow, enhanced backscattering cone, centered around the exact backscattering direction, and increasing by very nearly a factor of two at its peak. This enhanced backscattering results from the constructive interference of the electric fields of light paths traveling through the medium, following time-reversed paths. Similar effects are predicted for electrons, and, by analogy with the case of electrons, the enhanced backscattering cone is called “weak” localization of light. Since its observation, a great deal of effort has been expended in the search for “strong” localization of light. In this case, light would not be able to propagate because of the very strong scattering and hence would be localized. To date, however, strong localization of light due to intense multiple scattering has not been observed.

The main reason why light localization is so difficult to observe is that, perhaps surprisingly, very few media scatter light sufficiently strongly. In fact, one feature that emerges from virtually all of these studies is that the propagation of light in strongly scattering media can be described very well by the diffusion approximation. Within this approximation, all the effects of the interference of the fields within the medium are neglected, as it is assumed that the phases of all the photons are completely randomized [3]. Instead, only the intensity of the propagating light is considered. Moreover, since the light is scattered a large number of times, the path of the light is also completely random, and can be approximated by a random walk. The continuum limit of this description is the diffusion equation. The diffusion approximation is an adequate description of the light propagation, even in the case of enhanced backscattering, and can be used to determine the number and distribution of the time-reversed paths [4]. All the interference which leads to the enhanced cone occurs outside the medium, at the detector.

While the observation of “strong” localization of light remains elusive, the applicability of the diffusion approximation to describe the propagation of light can be exploited to learn new information about the scattering medium itself. It provides a simple and effective means of determining the distribution of light paths that photons follow on propagating through the medium. One very useful method of exploiting this knowledge is in the study of the dynamics of the scattering medium. These dynamics lead to temporal fluctuations of the scattered light, and their analysis can provide new information about the scattering medium, leading to a new technique for the study of the dynamics of strongly scattering media. This technique is called diffusing wave spectroscopy (DWS) and represents the extension of traditional dynamic light scattering (DLS) to strongly scattering media. This paper presents a brief review of the theory of DWS and a short discussion of some of its applications. The emphasis of the discussion of theory is on the physical concepts underlying its development, rather than the formal mathematics, which have been presented elsewhere. Furthermore, the emphasis of the discussion of its applications is on the novel physics that can be studied with DWS.

2. Theory

2.1. Non-interacting particles

In DWS, just as in conventional DLS, we measure the temporal fluctuations of the intensity in a single speckle spot of

the scattered light, or in a single spatial coherence area. We parameterize these fluctuations by their temporal autocorrelation function [5], $g_2(t)$. This is related directly to the autocorrelation function of the scattered electric fields, $g_1(t)$, which is a simpler quantity to calculate. We begin by discussing a system of noninteracting particles, and consider a colloidal suspension made up of identical, spherical particles, suspended in a fluid. In the limit of very low concentration, the self diffusion coefficient of these particles is given by the Stokes–Einstein relationship,

$$D_0 = \frac{k_B T}{6\pi\eta a}, \quad (1)$$

where k_B is Boltzmann's constant, T is the temperature, η the viscosity of the fluid, and a the particle radius. It is also convenient to define a characteristic time scale for diffusion of these particles by $\tau_0 = 1/k_0^2 D_0$, where $k_0 = 2\pi n/\lambda$, with n the index of refraction of the medium and λ the wavelength of the light in vacuum. This is the time it takes for a particle to diffuse the wavelength of light.

To analyze the data obtained with DWS requires the calculation of the autocorrelation function of the multiply scattered light [6, 7]. This is calculated by dividing the photons into separate, diffusive paths. The distribution of these paths, and the probability that a photon will follow a path of length, s , is determined through the use of the diffusion equation for the light. The contribution of each path to the total correlation function is calculated, taking advantage of the long length of the path, and the concomitant large number of scattering events [8]. The total correlation function is determined by summing the contributions of all possible paths, weighted by their probabilities. If the scattering particles in each path are completely uncorrelated, we need consider only the contribution of an individual path. These can then be added, assuming that all interference that contributes to the final signal comes only outside the sample, at the detector.

We begin by determining the correlation function of an n th-order path, consisting of n scattering events [8]. Since the number of scattering events is large, we approximate each event by an average scattering event, and neglect the conservation of momentum at each step. The scattering events are all independent, so the total correlation function is simply the product of n correlation functions of single scattering events, but each averaged over scattering angle so as to reflect the average scattering event in the path. This gives,

$$g_1^n(t) = \langle e^{-i\mathbf{q} \cdot \Delta\mathbf{r}(t)} \rangle_q^n, \quad (2)$$

where the subscript q refers to an average over all scattering vectors, weighted by the scattering probability or form factor. At short times, we can use a cumulant expansion and bring the ensemble average to the exponent. Furthermore, for each scattering event, the scattering vector is independent of the particle's mean square displacement, and each can be averaged independently, giving,

$$g_1^n(t) = e^{-n\langle q^2 \rangle_q \langle \Delta r^2(t)/6 \rangle}, \quad (3)$$

where again the subscript q indicates an average over scattering vectors. Finally, we identify the path length as $s = nl$, where l is the scattering mean free path of the light. Then,

we use the relationship [4],

$$\frac{l}{l^*} = \frac{\langle q^2 \rangle}{2k_0^2}, \quad (4)$$

for $\langle q^2 \rangle$, where l^* is the transport mean free path, the distance over which a photon must travel before its direction is randomized. For noninteracting, diffusion particles, $\langle \Delta r^2(t) \rangle = 6D_0 t$. We can further simplify the expression by introducing the characteristic time scale, $\tau_0 = 1/k_0^2 D_0$. Then we obtain

$$g_1^n(t) = e^{-2(t/\tau_0)(s/l^*)}. \quad (5)$$

The autocorrelation function does not depend on the scattering length, l , but only on the transport mean free path, l^* . This allows the diffusion equation for the light, which also depends only on l^* , to be used. The expression in eq. (5) has a simple physical significance: The first part of the exponent, $2t/\tau_0$, reflects the decay of the correlation function due to a single scattering event but averaged over all scattering vectors, weighted by the form factor of the particle. The additional quantity, s/l^* , reflects the effects of the multiple scattering. In following this diffusive path, the light is scattered through $n^* = s/l^*$ randomizing steps. It is only steps of order l^* that can lead to decay of the correlation function, as a single scattering step, of length l , is insufficient to change the direction of the light. Thus the decay rate of the total path is increased by a factor of n^* . Physically, the decay of this correlation function reflects the time it takes for the total path length to change by a wavelength. This change results from the cumulative motion of a large number of particles. Thus long paths decay more rapidly since they are scattered from a larger number of particles, and each individual particle must move a shorter distance, and hence take a shorter time, for the cumulative path length to change by a wavelength. By contrast, shorter paths decay more slowly as the light is scattered by fewer particles and each individual particle must move a relatively larger distance, and hence take a larger time, before the total path changes by a wavelength. We note, however, that the correlation function for each path has a linear dependence in the exponential on both the path length, s , and on time, t .

To obtain the full autocorrelation function, we sum over the contributions from all paths, weighted by the probability $P(s)$, that the light follows the path,

$$g_1(t) = \int_0^\infty P(s) e^{-2(t/\tau_0)(s/l^*)} ds. \quad (6)$$

With this expression, we implicitly assume that each path is uncorrelated with other paths and thus simply add the contributions of the different paths. The quantity $P(s)$ depends explicitly on the geometry of the experiment, but can be determined through the use of the diffusion equation for the light. The method of its determination can be physically understood by considering what happens to a very narrow pulse of light incident on one side of the scattering medium. This light must travel roughly l^* into the medium before it has scattered a sufficient number of times that its transport becomes diffusive. The pulse exiting from the other side will reflect the distribution of paths followed by the diffusing photons. Some of the photons will follow very short paths and will exit the sample after a short time. Many more of

the photons will follow longer paths and will be delayed before they exit. Some photons will follow very long paths and will exit much later. Thus, the pulse that exits the other side of the sample will exhibit considerable dispersion. Since the speed of light in the medium, c , is known, the dispersion in time of the transmitted pulse directly reflects the distribution of paths the light takes in passing through the medium. This allows $P(s)$ to be determined.

The diffusion equation can be solved for the geometry of the experiment to actually calculate the path distribution, $P(s)$. Since it is a partial differential equation, the boundary and initial conditions must be specified. The boundary conditions are chosen to ensure that there is no flux of diffusing photons into the sample at the boundaries [9, 10]. The initial conditions are chosen to provide a delta function in time of diffusing photons, a distance l^* into the sample on the side that the laser is incident. We then solve the diffusion equation to obtain the flux of diffusing photons emitted from the sample at the detector, and use the transformation, $s = ct$ to obtain $P(s)$. In fact the solution for the autocorrelation function is actually somewhat simplified by recognizing that eq. (6) is the Laplace transform of $P(s)$, so that we need only obtain the solution to the Laplace transform of the diffusion equation to recover the autocorrelation function directly.

The correlation function measured with DWS can be calculated for several experimentally relevant geometries [6, 7, 11, 12]. Here, we consider the case where the light is transmitted through the sample, which we take to be a slab of infinite extent and of thickness, L . If the incident laser is focused to a point on one side of the sample, and the scattered light is collected from a point on the other side of the sample, on the same axis as the incident light, the normalized field correlation function is given by,

$$g_1(t) = \int_{(L/l^*)\sqrt{6t/\tau_0}}^{\infty} [A(s) \sinh s + e^{-s(1-4l^*/3L)}] ds, \quad (7)$$

where

$$A(s) = \frac{\left(\frac{2l^*}{3L}s - 1\right) \left[\frac{2l^*}{3L} e^{-4sl^*/3L} + \left(\sinh s + \frac{2sl^*}{3L} \cosh s \right) e^{s(1-4l^*/3L)} \right]}{\left(\sinh s + \frac{2sl^*}{3L} \cosh s \right)^2 - \left(\frac{2sl^*}{3L} \right)^2} \quad (8)$$

If the incident laser beam is expanded to fill the full surface of the sample, the autocorrelation function is obtained by integrating over all the point sources on the incident side. This yields a closed form rather than an integral,

$$g_1(t) = \frac{\left(\frac{L}{l^*} + \frac{4}{3}\right) \sqrt{\frac{6t}{\tau_0}}}{\left(1 - \frac{8t}{3\tau_0}\right) \sinh \left[\frac{L}{l^*} \sqrt{\frac{6t}{\tau_0}} \right] + \frac{4}{3} \sqrt{\frac{6t}{\tau_0}} \cosh \left[\frac{L}{l^*} \sqrt{\frac{6t}{\tau_0}} \right]} \quad (9)$$

In either case, the form of the autocorrelation function is nearly exponential, and the characteristic decay time is $\tau_0(l^*/L)^2$. While complicated, these expressions are readily evaluated, and provide excellent agreement with the data.

2.2. Interacting particles

Since DWS is ideally suited for the study of very concentrated suspensions, it is also essential to consider the correlation function for a suspension of strongly interacting particles. We can do this by analogy to the case of noninteracting particles [13, 14]. We again consider an n th-order diffusive light path. The correlation function is once again the product of n independent, single scattering correlation functions, averaged over scattering angle. However, now these individual correlation functions must now include the effects of the particle interactions on the light scattering. We therefore rewrite eq. (2) as

$$g_i^n(t) = \frac{\langle F(q)S(q, t) \rangle_q^n}{\langle F(q)S(q) \rangle_q^n}, \quad (10)$$

where $S(q, t)$ is the dynamic structure factor that describes the light scattering from the suspension. To express this in a form suitable for use with the diffusion equation to describe the propagation of the light, we expand the dynamic structure factor at short times,

$$S(q, t) \approx S(q) \left[1 - \frac{q^2}{6S(q)} W(q, t) \right], \quad (11)$$

where we will define the meaning $W(q, t)$ later. We first use eq. (11) to put eq. (10) into a form that is suitable for use in the Laplace transform of eq. (6). This can be accomplished by making a cumulant expansion of eq. (10),

$$g_i^n(t) \approx \left[1 - \frac{\frac{1}{6} \langle q^2 F(q) W(q, t) \rangle_q}{\langle F(q)S(q) \rangle_q} \right]^n, \quad (12)$$

and then by again restricting ourselves to short times and replacing eq. (12) by the exponential,

$$g_i^n(t) \approx e^{-n \langle q^2 F(q) W(q, t) \rangle_q / 6 \langle F(q)S(q) \rangle_q}. \quad (13)$$

We emphasize here that the averages over q in both eqs (12) and (13) must now be performed while taking into account the interactions of the particles, and their effect on the light scattering. Finally, to express eq. (13) in a form suitable for use with the diffusion equation for light we re-express the denominator of the exponent using the relationship between the scattering and transport mean free paths for interacting particles [4, 7],

$$\frac{l}{l^*} = \frac{\langle q^2 F(q)S(q) \rangle_q}{2k_0^2 \langle F(q)S(q) \rangle_q} \quad (14)$$

From this, we obtain the normalized field autocorrelation function for n th-order paths,

$$g_i^n(t) \approx e^{-2k_0^2 (s/l^*) \langle q^2 F(q) W(q, t) \rangle_q / 6 \langle q^2 F(q)S(q) \rangle_q} \quad (15)$$

Here s is the length of the path, while l^* is the transport mean free path for the interacting system. This expression for the correlation function for n th-order paths is now suitable for use directly in the Laplace equation that describes the full correlation function, eq. (6). Moreover, the results obtained for the transmission geometries, eqs (7), (8) and (9), can be used directly for interacting systems as well, by substituting t/τ_0 by $\langle q^2 F(q) W(q, t) \rangle_q / 6 \langle q^2 F(q)S(q) \rangle_q$. Thus, for interacting system, DWS measures an average over q of $W(q, t)$, weighted by $q^2 F(q)$.

To make use of this result, we expand the dynamic structure factor for short times and thereby determine $W(q, t)$.

The dynamic structure factor is

$$S(q, t) = \frac{1}{N} \left\langle \sum_{j, k=1}^N e^{-i\mathbf{q} \cdot [\mathbf{r}_j(t) - \mathbf{r}_k(0)]} \right\rangle \quad (16)$$

where $\mathbf{r}_i(t)$ is the position of the i th particle at time t , and the summation extends over N particles. To expand this for short times we first use a theorem valid for ergodic systems, where the time and ensemble averages are equivalent,

$$\frac{d^2}{dt^2} \langle \mathbf{A}(0) \cdot \mathbf{B}(t) \rangle = -\langle \dot{\mathbf{A}}(0) \cdot \dot{\mathbf{B}}(t) \rangle. \quad (17)$$

Substituting the dynamic structure factor in this equation, we obtain

$$\frac{d^2}{dt^2} S(q, t) = -\frac{1}{N} \sum_{i, j=1}^N \langle \mathbf{v}_i(0) \cdot \mathbf{v}_j(t) e^{-i\mathbf{q} \cdot [\mathbf{r}_i(t) - \mathbf{r}_j(0)]} \rangle \quad (18)$$

where $\mathbf{v}_i(t)$ is the velocity of the i th particle at time t . This enables us to express the dynamic structure factor in terms of the velocities of the particles. At very short times, the particles have not moved significantly from their positions at $t = 0$, so the quantity in the square brackets in the exponential can be replaced by its initial value, $\mathbf{r}_{ij} = \mathbf{r}_i(0) - \mathbf{r}_j(0)$. In making this approximation, we assume that the correlations in the structure of the particles change much more slowly than the time scale of the particle motion being probed by DWS. Equation (18) can then be written as

$$\frac{d^2}{dt^2} S(q, t) = -\langle \mathbf{v}(0) \cdot \mathbf{v}(t) \rangle - \frac{1}{N} \sum_{i \neq j}^N \langle \mathbf{v}_i(0) \cdot \mathbf{v}_j(t) e^{-i\mathbf{q} \cdot \mathbf{r}_{ij}} \rangle, \quad (19)$$

where we have split the summation into two parts, the self part, where $i = j$, and the distinct part, where $i \neq j$. The first term is the velocity autocorrelation function of single particles, and reflects the self-diffusion of the particles, whereas the second term involves the correlations between velocities of different particles. To obtain $S(q, t)$ at short times, we integrate eq. (19) twice giving

$$S(q, t) \approx S(q) \left[1 - \frac{q^2}{6S(q)} \left\{ \langle \Delta \mathbf{r}^2(t) \rangle + \frac{1}{N} \sum_{i \neq j}^N \langle \Delta \mathbf{r}_i(t) \Delta \mathbf{r}_j(t) e^{-i\mathbf{q} \cdot \mathbf{r}_{ij}} \rangle \right\} \right], \quad (20)$$

from which we define

$$W(q, t) = \langle \Delta \mathbf{r}^2(t) \rangle + \frac{1}{N} \sum_{i \neq j}^N \langle \Delta \mathbf{r}_i(t) \Delta \mathbf{r}_j(t) e^{-i\mathbf{q} \cdot \mathbf{r}_{ij}} \rangle \quad (21)$$

and obtain the desired expansion for $S(q, \tau)$, used in eq. (11). Diffusing wave spectroscopy provides a measure of $W(q, t)$ defined in eq. (21). This measure is, as always with DWS, an average over q , weighted by $q^2 F(q)$.

To better appreciate the physical significance of $W(q, t)$, it is useful to consider its behavior in some limiting cases. First, we consider the situation of noninteracting particles, in which case $S(q) = 1$ and the second term of eq. (21) does not contribute because the value of \mathbf{r}_{ij} is always sufficiently large compared to that of \mathbf{q} to ensure that the summation over the exponential averages to zero. Then $W(q, t) \approx \langle \Delta \mathbf{r}^2(t) \rangle$, and is simply the mean square displacement of the particles. At longer times, the expansion of the dynamic structure factor must reduce to the more familiar form that was originally developed for single scattering from inter-

acting systems [15], and $W(q, t) = D_0 H(q)$, where $H(q)$ reflects the effects of hydrodynamic interactions. In this case, DWS probes quantities that are analogous to the case of DLS in the single scattering limit. We recall that DLS from interacting particles measures $D_{\text{eff}}(q) = D_0 H(q)/S(q)$. By comparison, DWS measures the same quantities, but averaged over q , and weighted by $q^2 F(q)$ [16, 17],

$$D_0 \frac{\langle q^2 F(q) H(q) \rangle_q}{\langle q^2 F(q) S(q) \rangle_q}.$$

We note that the evaluation of the average over q entails the integration,

$$\langle q^2 F(q) X(q) \rangle_q = \int q^3 F(q) X(q) dq.$$

This results in a factor of q^3 weighting the integral; a factor of q^2 because DWS is sensitive to the motion of the particles, and a factor of q to properly average over phase space. As a result, this average is heavily weighted towards the contributions at the larger values of q .

While the approximation using $H(q)$ is often adequate, the reason for performing the expansion in terms of the velocity correlation functions is that DWS can, in principle, probe particle motion at sufficiently short length scales, and hence time scales, that the time dependence of $H(q)$ must be considered. When this must be done, we can still consider two different cases, both using eq. (21) for $W(q, t)$. In the first case, when the particles are large, the summation in eq. (21) again averages to zero, and $W(q, t)$ reduces to the mean square displacement. Physically, the particles are so large that only a single particle can fit into the average volume of a scattering event, which is roughly $\langle q \rangle^{-3}$, and DWS is sensitive only to the motion of the individual particles, or the self-diffusion coefficient. This is analogous to the case of DLS from large particles, which is also sensitive only to the self diffusion coefficient, even for interacting particles [15]. It is only in the case of small particles that the full form of eq. (21) must be used. Then DWS is sensitive to a combination of the self diffusion coefficient of the particles, as well as a term that reflects the relative motion of neighboring particles. In this case, more than one particle fits into the volume probed by a scattering event, and both the motion of the individual particles and their relative motion affect the light scattering. This is again analogous to the situation of DLS, which measure collective diffusion if the particles are sufficiently small compared to q^{-1} . Thus DWS measures quantities that are very similar to DLS, but are averaged over q and weighted by $q^2 F(q)$.

3. Applications

3.1. Non-interacting systems

We first investigate DWS from non-interacting systems, and test the expressions for transmitted light, eqs (7), (8) and (9). In Fig. 1, we plot the intensity autocorrelation functions measured in transmission for both a point source and an expanded source. The data are obtained from a 1 mm thick sample of uniform polystyrene latex spheres of diameter $d = 0.605 \mu\text{m}$ with a volume fraction of $\phi = 2.1\%$. The incident laser had a wavelength of $\lambda = 488 \text{ nm}$ *in vacuo*. The upper data set in Fig. 1 was obtained with the incident laser

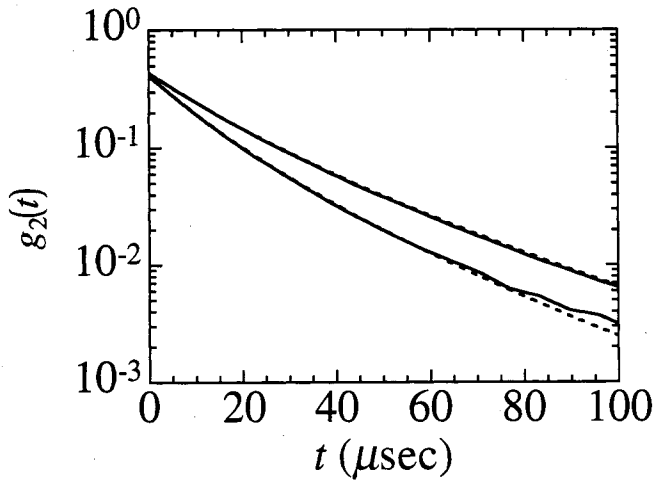


Fig. 1. Intensity autocorrelation functions measured in transmission for point source illumination (upper curve) and extended source illumination (lower curve), compared with the theoretical fits (dashed lines). The same value of l^* is obtained from each geometry.

focused to a point, while the lower data set was obtained with the laser beam expanded to a diameter of ~ 1 cm. The data obtained with the expanded laser source clearly decay more rapidly than those obtained with the point source, as expected, reflecting the larger contribution of longer paths when the source is expanded. The value of τ_0 can be calculated, or measured using conventional DLS from a dilute sample, and is $\tau_0 = 4.88$ msec. Then the only unknown quantity in eqs (7), (8) and (9) is the value for the transport mean free path. We therefore fit the point source data to eqs (7) and (8), and the expanded source data to eq. (9) using l^* as a fitting parameter. The results are shown by the dashed lines, and are in excellent agreement with the data. Furthermore, we obtain $l^* = 166 \mu\text{m}$ from the fit to the point source data, and $l^* = 167 \mu\text{m}$ from the fit to the expanded source data. The excellent consistency between the two values confirms the validity of the theoretical interpretation.

One unique feature of DWS is its sensitivity to particle motion on very short length scales. In transmission, there is always a characteristic length for the diffusive paths of the light, and this length can be experimentally controlled through the variation of the sample thickness. The fluctuations of the scattered light measured in transmission result from the variation of the total path length by a wavelength of light. However, since the light is scattering from a large number of particles, each individual particle must move only a small fraction of a wavelength for the cumulative change in the path length to be a full wavelength. Thus DWS can measure particle motion on very short length scales. The typical number of scattering events contributing to a path in transmission is $n^* = (L/l^*)^2$. For the path length to change by a wavelength, the average root mean square displacement of each individual particle must be roughly $\lambda/(n^*)^{1/2}$. Since n^* can easily be greater than 10^4 , and since we can easily detect the change of a path length by a tenth of a wavelength, DWS can measure motions of particles of order $1 \mu\text{m}$ in diameter on length scales of less than 1 nm .

To demonstrate the sensitivity of DWS to motion on very short length scales, we use polystyrene latex spheres in water [18]. The ionic strength of the water is sufficiently high that the screening length is very short and the particles interact as hard spheres. To simplify the interpretation, we

use $1.53 \mu\text{m}$ diameter spheres, allowing the DWS data to be expressed in terms of the mean square displacement of individual particles. We use a sample with a volume fraction of $\phi = 2.1\%$, which is low enough that the effects of hydrodynamic interactions are negligible. The sample is held in a 1 mm thick cuvette, which is immersed in a water bath thermostated to $\pm 0.1^\circ\text{C}$ during the measurement. To obtain very high speed data, it is essential to avoid the deleterious effects of the spurious correlations from after pulsing in the photo-multiplier tube (PMT), and from the dead time in the detection electronics. The negative effects of both of these are reduced by using a fiber-optic beamsplitter after the final pinhole in the detection optics, which directs equal portions of the light onto two PMTs. The signals of these are cross correlated [19], extending the measurements to the shortest sample time available on the correlator, 12.5 nsec . In addition, we use an intercavity etalon to force the laser to operate on a single longitudinal mode, thereby avoiding detection of the beats between the output from adjacent modes. The etalon also ensures that the coherence length of the exciting laser is much longer than the longest paths contributing to the DWS signal in transmission, avoiding any distortions in the shape of the autocorrelation function. To obtain good statistics for the autocorrelation functions at the shortest delay times requires extensive signal averaging. Thus, data are collected for a total of about 12 hours. Rather than collecting a single data set, we measure the autocorrelation function for 10 minutes, and then rotate the sample to eliminate any gravitational settling. Finally, all the data sets are summed to obtain the desired autocorrelation function.

The data are analyzed to obtain the root mean square displacement of the particles. This is done by using a zero-crossing routine to invert the measured autocorrelation function assuming the functional form of eq. (7), and using the value of l^* calculated with Mie theory. The results are shown in Fig. 2, where we plot $\langle \Delta r^2(t) \rangle^{1/2}$, measured in Ångströms, as a function of time. Particle motion on length scales as short as 2 Å can be clearly detected. This is a dramatic demonstration of the power of DWS to resolve motion on very short length scales.

In addition to the transmission geometry, the formalism for DWS can also be developed for the backscattering geometry [6, 7, 20]. In this case, the laser beam must be

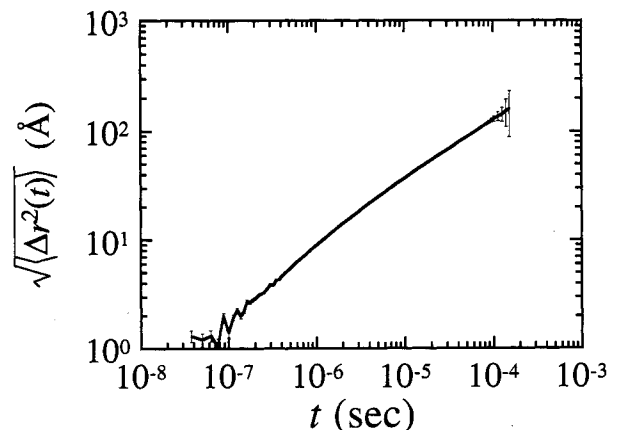


Fig. 2. Root mean square displacement as a function of time for $1.53 \mu\text{m}$ particles, showing the sensitivity of DWS to motions on very short length scales.

expanded to fill a large area of the surface of the sample, and the backscattered light must be collected from a small spot at the center of the incident beam. As is the case for transmission, the exact angle of collection is not essential, since the multiply scattered light exits in all directions. Unfortunately, the interpretation of the backscattering results is not as clear as it is for the transmission geometry. In transmission, the autocorrelation function is dominated by diffusive light paths of a characteristic length, determined by the diffusive transmission through the sample. By contrast, in backscattering, paths of all lengths contribute. In particular, there is a large contribution of very short paths, where the light is scattered a small number of times before exiting the sample and coming back to the detector. The length of these paths can easily be comparable to the transport mean free path, for which the diffusion approximation is no longer adequate. The exact treatment of the contribution of these paths is beyond the diffusion theory developed here. Thus, while the theory gives excellent qualitative agreement with the data, quantitative correspondence cannot be achieved.

3.2. Transient hydrodynamic interactions

At the very short time scales probed by DWS, the motion of Brownian particles is no longer simply diffusive. Instead, at these time scales, it is possible to directly probe the decay of the velocity autocorrelation function, $R(t) = \langle v(t)v(0) \rangle$, of the particles [21]. The decay of the velocity autocorrelation function reflects the consequences of the motion of the fluid around the particles and the interactions of the particle with the surrounding fluid. The velocity autocorrelation function is the second derivative of the mean square displacement, and to determine it, we numerically calculate the second derivative of the measured data for $\langle \Delta r^2(t) \rangle$. This is accomplished by fitting the results around each data point to a third order polynomial and calculating the first and second derivatives from the fit. In Fig. 3, we show the results for the second derivative of the data for the mean square displacement shown in Fig. 2. We observe a power law decay of the velocity autocorrelation function, with $R(t) \sim t^{-3/2}$, as indicated by the solid line in Fig. 3. The origin of this power-law behavior is the frequency dependence of the interaction between the particle and the fluid [22]. Physically, as the

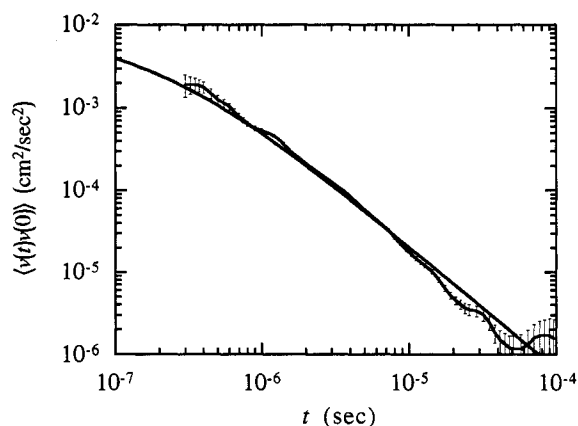


Fig. 3. Velocity autocorrelation function of $1.53\ \mu\text{m}$ diameter particles determined from the second derivative of their mean square displacement. The theoretical prediction is shown by the solid line.

particle moves, it must push the fluid out of its way, setting up a wake as the fluid flows around it. The fluid flow acts back on the particle pushing it in the same direction that it is moving, causing the velocity of the particle to persist for a longer time. This results in the power-law form of the decay of the velocity autocorrelation function. This behavior is common to all velocity autocorrelation functions of particles moving in an environment where hydrodynamics are important. It was predicted in computer simulations of hard sphere fluids [23], and is known as the “long-time” tail of the velocity autocorrelation function. It results from the fact that the fluid must also move, in addition to the particle. The time scale for changing the fluid velocity is determined by the viscosity, and is $\tau_H = a^2\rho/\eta$. This is the time scale for the vorticity to diffuse a distance set by the particle radius. The functional form for the velocity autocorrelation function can be obtained by solving the Langevin equation with a time dependent friction coefficient, reflecting the hydrodynamic memory effects due to the fluid flow [22]. Then, the $t^{-3/2}$ “long-time” tail in $R(t)$ is correctly predicted. The predicted results are in excellent accord with the measurements, as shown by the solid line through the data in Fig. 3, which is the theoretical calculation. We emphasize that there are no fitting parameters used in obtaining the fit. The time scale is set by the particle radius, density and the fluid viscosity, all of which are known independently. The length scale determined by DWS is set by the sample thickness and the wavelength of light, both of which are known, and by the transport mean free path, which is calculated theoretically from Mie theory. These results are a clear illustration of the power-law “long-time” tail in $R(t)$. They illustrate the power of DWS in following the time evolution of hydrodynamic interactions. The “long-time” tail of the velocity correlation has been observed, with great difficulty, using DLS [24]; with DWS, it becomes possible to study the retarded, or transient, nature of hydrodynamic interactions with much greater ease and clarity.

As the particle concentration increases, the fluid flow around the particle will be modified by the presence of the neighbors. We can probe the consequences of these modifications using DWS. The modification of the motion of one particle due to the change in the fluid flow field caused by the presence of a second particle is a direct manifestation of hydrodynamic interactions. Thus DWS can provide new insight into the nature of these hydrodynamic interactions. In particular, we are able to measure the time evolution of hydrodynamic interactions as the fluid flow evolves. Physically, we expect many body hydrodynamic interactions to be important as the vorticity of the fluid diffuses away from the tracer particle and the flow pattern is interrupted by the neighboring particles. The flow field will cause the neighboring particles to move, which will result in an additional flow field which will, in turn, modify the motion of the tracer particle. This interaction will not be instantaneous because the diffusion of the vorticity between particles requires some time. An estimate of this time scale is $\tau_n \approx s^2\rho/\eta$, where s is the mean surface to surface distance between neighboring particles. As the volume fraction goes up, this time scale should decrease, and hydrodynamic interactions should become more important.

To investigate the transient hydrodynamic interactions, we repeat the same transmission measurements using differ-

ent volume fractions of the $1.53\ \mu\text{m}$ diameter spheres. Instead of plotting $\langle\Delta r^2(t)\rangle$, it is more informative to consider the time-dependent self-diffusion coefficient. However, rather than introducing additional numerical inaccuracy by differentiating the data, we instead define $D(t) \equiv \langle\Delta r^2(t)\rangle/6t$. We plot the time-dependent self-diffusion coefficients measured for several volume fractions in Fig. 4. For comparison, we also plot, by the dashed line, the theoretically predicted behavior for zero volume fraction, using the full, time-dependent viscosity [22]. The data for the lowest volume fraction, $\phi = 2.1\%$, is indistinguishable from the theoretically predicted behavior at zero volume fraction. As the volume fraction increases, the data deviates from the zero volume fraction limit by greater amounts and at apparently earlier times. The asymptotic value for each data set decreases as the volume fraction increases, although we are not able to follow the data to sufficiently long times to observe the true asymptotic behavior, despite the fact that our measurements extend to approximately $100\tau_H$. Thus the very slow approach to the asymptotic behavior that gives rise to the "long-time" tail of the velocity autocorrelation function of the zero-volume fraction data is also apparent for higher volume fractions.

The velocity autocorrelation functions determined from the data for the higher volume fractions also each exhibit a $t^{-3/2}$ behavior. To quantify this behavior, we fit the data to the functional form for low volume fractions, using both the asymptotic self-diffusion coefficient and the viscous time scale as fitting parameters. For each volume fraction, an excellent fit is obtained. Thus the data exhibit a remarkable scaling behavior and can all be plotted together onto a single master curve, as shown in Fig. 5. The shape of this master curve is described by the functional form of the theory for low volume fractions, as shown by the solid line in Fig. 5. Data obtained with $3.1\ \mu\text{m}$ diameter spheres also exhibit the same scaling behavior.

The scaling of the data onto a single master curve provides two different scaling parameters. The first is the value of the self-diffusion coefficient required to scale the data on the vertical axis. This value corresponds to the asymptotic value of the self-diffusion coefficient at longer times, after the transient nature of the hydrodynamic interactions has subsided, but before the particle positions have changed substantially, and thus before the longer time behavior of

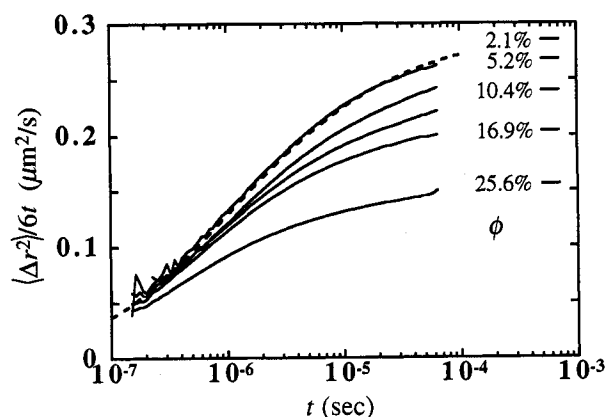


Fig. 4. Time-dependent self-diffusion coefficients for different volume fractions of $1.53\ \mu\text{m}$ diameter spheres, showing the very slow approach to the asymptotic values, which are shown by the lines on the right. The theoretical prediction for zero volume fraction is shown by the thick line.

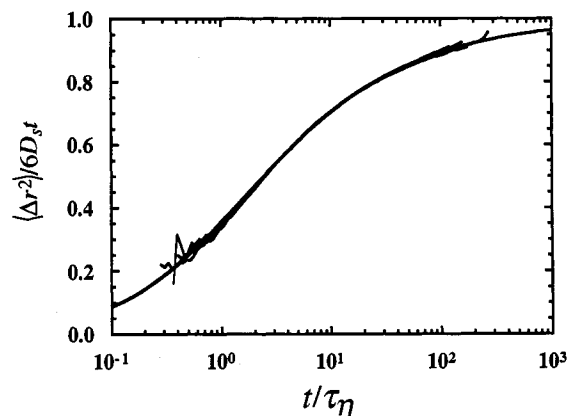


Fig. 5. Scaling of the time-dependent self-diffusion coefficients for different volume fractions of the $1.53\ \mu\text{m}$ diameter spheres. Each data set has been normalized by its asymptotic value of D_s and is plotted as a function of time normalized by the new viscous time, τ_η .

the self-diffusion coefficient becomes apparent. Thus the value of this scaling parameter corresponds to the short-time self-diffusion coefficient and can be compared with both theoretical predictions [25, 26] and with measurements using single scattering from tracer particles in index matched suspensions [27, 28]. We find good agreement between our data and these previous measurements, with the asymptotic value of the self-diffusion coefficient decreasing approximately as $(1-1.83\phi)$ from its value at zero volume fraction. The second parameter is the time required to scale the data on the horizontal axis. The volume fraction dependence of this new, viscous time scale, normalized by its zero volume fraction limit, is plotted in Fig. 6. We show data obtained with both the $1.53\ \mu\text{m}$ diameter spheres (diamonds), and with $3.09\ \mu\text{m}$ diameter spheres (circles). The time scale also decreases with increasing volume fraction, but does so at a faster rate than the self-diffusion coefficient. Since the viscous time scale is inversely proportional to the viscosity, we also plot, by the solid line, the volume-fraction dependence of the inverse of the theoretically predicted viscosity for a hard-sphere suspension, normalized by the viscosity of the solvent [29]. The data are described remarkably well by the theoretical behavior. We emphasize

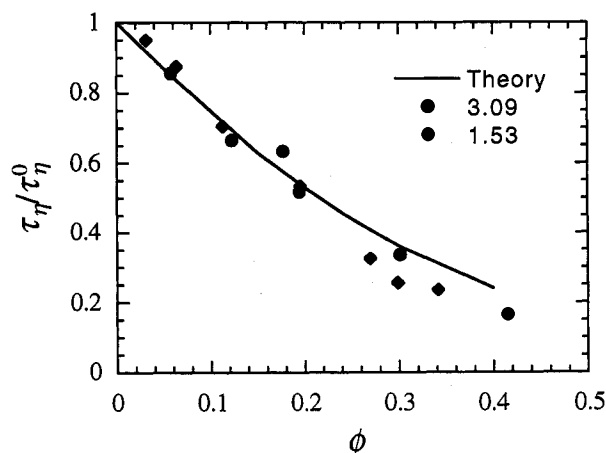


Fig. 6. Scaling time for different volume fractions of $1.53\ \mu\text{m}$ diameter spheres (diamonds) and $3.09\ \mu\text{m}$ diameter spheres (circles), normalized by their zero-volume fraction time. The solid line is the theoretical prediction of the volume fraction dependence of the inverse of the viscosity of the suspension.

again, however, that the ϕ -dependence of the two scaling parameters is notably different; the value of the scaling time decreases significantly more rapidly with increasing volume fraction than does that of the asymptotic self-diffusion coefficient.

The data presented here show that the time evolution of the self-diffusion coefficient has a remarkable, universal form, independent of volume fraction. For all values of ϕ , the velocity autocorrelation function exhibits a “long-time” tail, and an algebraic decay, with a $t^{-3/2}$ time dependence. Thus the observations presented here show that the “long-time” tail in the velocity autocorrelation function is a very general feature of fluids, occurring in a very similar fashion for fluids composed of very different components. The scaling of the data, and the ϕ -dependence of the viscous time scale suggest a simple physical picture for the behavior. At long times, the vorticity has diffused a sufficiently large distance, so that the fluid flow can no longer distinguish the individual particles in the suspension, which instead appears as an average medium. This suggests that an effective medium approach may be a useful approximation for describing the behavior of hydrodynamic interactions at these time scales.

While the scaling behavior reported here does suggest a simple physical picture, the underlying origin of the behavior is not yet understood. The behavior at longer times is apparently determined by the viscous time constant of the suspension. However, it is surprising that the observed scaling applies so well at relatively short times, well before the vorticity has diffused over many particle diameters. The data shown in Fig. 5 indicate that the scaling behavior extends to times as short as $t \sim 0.5\tau_H$, which is much earlier than expected from a physical picture of the diffusion of the vorticity between neighboring particles. At these very shortest times, we might expect the time-dependent self-diffusion coefficient to be independent of volume fraction, as the vorticity will not have diffused far enough for the flow field to be disrupted by the neighboring particles. At these very short times, the scaling behavior should not be observed if the unscaled data were identical. However, this time scale might be very short, even shorter than we can observe in our experiments, since in a hard sphere suspension, there is no characteristic particle separation and some particles are separated by distances much smaller than the average separation.

Although a fundamental theoretical understanding is lacking as yet, considerable guidance can be obtained from recent computer simulations [30]. These use a new form of a lattice gas model to describe the hydrodynamic interactions between the particles. The simulations are performed with a lattice Boltzmann model, to which is added random noise to simulate the Brownian fluctuations. With this model, it is possible to determine the particle mean free displacement at early times, corresponding to the time scales measured here. Exactly the same scaling behavior for the time dependent self diffusion coefficient is found in the simulations. Moreover, the two scaling parameters are different, and have different dependencies on the volume fraction of particles. The ϕ -dependencies observed in the simulations are identical to those observed in these experiments. Finally, with the simulations, it is possible to extend the data to even shorter times than in the experiment. The same scaling

behavior persists to these very short times. Thus, these simulations provide further confirmation of the data. In addition, it should be possible to use the simulation results to assist in developing a better understanding of the underlying physics of the transient hydrodynamic interactions.

Additional information about the transient hydrodynamic interactions is obtained by using spheres with smaller diameters. In this case, more than a single sphere can fit into the average volume probed by each scattering event, $\langle q \rangle^{-3}$. Thus the second summation in $W(q, t)$, eq. (21), makes a contribution, making it possible to explore the temporal behavior of the interparticle hydrodynamic interactions, or the consequences of velocity cross correlations. To do this, we repeat the measurements of the correlations functions using spheres of diameters 0.76, 0.412 and 0.198 μm , at increasing volume fractions for each. The data are again inverted using the functional form of eqs (7) and (8). We then determine $\langle q^2 F(q) W(q, t) \rangle_q$ using the measured values of L and l^* and the value of $\langle q^2 F(q) S(q) \rangle_q$ calculated for hard spheres assuming a pair distribution function given by Percus–Yevick [31]. We define an effective time-dependent diffusion coefficient by $D_{\text{eff}} \equiv \langle q^2 F(q) W(q, t) \rangle_q / 6t$. The measured quantity is no longer simply interpreted as the mean square displacement because of the contribution of the second summation in eq. (21). However, the general behavior of these data is the same as that observed for the larger spheres. At very low volume fractions, the data follow the theoretical prediction, as they should, since the interactions are negligible at sufficiently low ϕ . Interestingly, however, as the particle size decreases, the volume fraction required to obtain agreement with the zero ϕ limit of the theory also decreases significantly. At higher volume fractions, deviations from the theoretical prediction are observed.

Very surprisingly, it is again possible to scale all the data onto the same universal curve, whose functional form is given by the time-dependent self-diffusion coefficient in the limit of zero volume fraction. The data obtained with the smaller spheres extend over a somewhat different range in reduced time since the particles are so much smaller. We probe times between about $2\tau_H$ and $200\tau_H$. The scaling of the data is an experimental observation; it is not at all clear why it should occur. In particular, since, from the measurements on the larger particles, we know that the first term in eq. (21) exhibits this scaling, it is unclear why the sum of the first term and a second term should scale the same way as the first term itself.

We again obtain two scaling parameters. The first reflects the ϕ -dependence of the asymptotic value of D_{eff} . The second reflects the new viscous time scale, and includes the influence of the second term in eq. (21), reflecting the effects of velocity cross correlations between neighboring particles. We plot the ϕ -dependence of this new time scale for all the smaller diameter spheres in Fig. 7. For comparison, we also show the behavior of the larger diameter spheres. For the spheres smaller than 0.76 μm in diameter, the time scales have a markedly different ϕ -dependence than do the larger spheres. The new time scale is always reduced by comparison to the results for the large spheres. Thus the effects of the velocity cross-correlations is to reduce the time scale compared to the behavior of the self-diffusion coefficient. Moreover, for the smallest spheres, we must go to very low volume fractions, $\phi \approx 0.5\%$, before the behavior reduces to

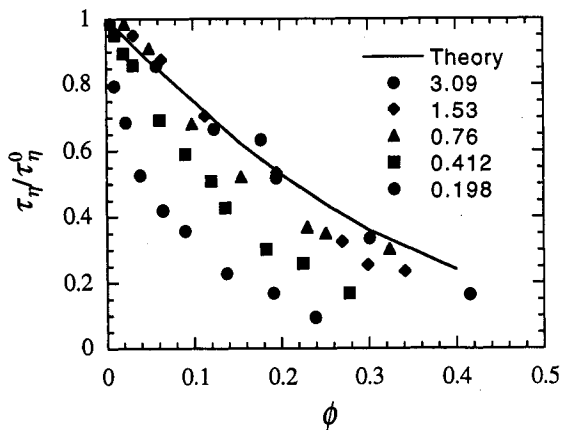


Fig. 7. Scaling time for different volume fractions of spheres with smaller diameters, including 0.76 (triangles), 0.412 (squares) and 0.198 μm (circles). These are compared with the behavior of the larger spheres, with diameters of 1.53 (diamonds) and 3.09 μm (circles). All the data sets have been normalized by their zero-volume fraction times. The solid line is the theoretical prediction of the volume fraction dependence of the inverse of the viscosity of the suspension.

the limit of non-interacting, or zero volume fraction, spheres. The fact that the scaling time differs for the smaller spheres reflects the contribution of the second term in eq. (21), and indicates the effects of the hydrodynamic interactions between neighboring spheres. The contribution of this effect increases as the size of the spheres decreases. The behavior observed here is to be contrasted with that observed by DWS at even shorter time scales, where the autocorrelation function was measured with a Michelson interferometer instead of a correlator [32]. These observations were performed on small spheres, with diameters less than 0.5 μm , but the data extend to much shorter time scales, ranging from about $0.1\tau_H$ to $1\tau_H$. Similar scaling behavior of the measured D_{eff} was observed, but the ϕ -dependence of the scaling time was notably different than the measurements presented here for time scales larger than τ_H . At very short times, the scaling time had the same ϕ -dependence as do the large spheres. Thus our results suggest that the effects of the velocity cross correlations do not begin to affect the results until times of order τ_H , implying that the transient nature of the hydrodynamic interactions between neighboring particles is very different than those interactions affecting the self-diffusion coefficient. Clearly, further work is required to fully interpret these results. Nevertheless, these data demonstrate the power of DWS to observe motion of particles on very short length scales and thereby probe new physical phenomena.

3.3. Foams

Another application for which DWS is ideally suited is the measurement of systems where the dynamics entail events that are both spatially and temporally rare. In this case, the fact that DWS is sensitive to the dynamics of a relatively large sample volume makes the measurement of the autocorrelation function much more feasible. As an example of this type of dynamics, we study shaving cream [33, 34], which is a prototypic foam, comprised of bubbles of gas, suspended in a fluid, and stabilized by surfactant molecules at the interfaces. Provided no coloring is added for cosmetic purposes, shaving cream is white, due to the very strong multiple scattering of light from the bubble interfaces. As

such, it is an ideal candidate for studying with DWS. The shaving cream we study is Gillette Foamy; it is a highly reproducible foam, with very low absorption of the light. The diffusion approximation describes the transport of light through Foamy very well.

The dynamics in shaving cream arise from the coarsening which occurs in the foam. In general, this coarsening can occur by two distinct mechanisms. In the first, two bubbles can approach and coalesce, forming a single larger bubble. By contrast, the second mechanism is analogous to Ostwald ripening. In this case, the coarsening results from the slight solubility of the gas in the fluid. Then the difference in the internal pressures of the bubbles provides the force which drives the gas from the smaller bubbles, which have a larger internal pressure, to the larger bubbles, which have a smaller internal pressure. In both cases, the net result is the disappearance of the smaller bubbles, so that the average bubble size increases in time. Coarsening is very generally observed in foams. At the same time, the total volume fraction of gas relative to the liquid remains constant in time. For most foams, this volume fraction is on the order of 90%, or greater; for Foamy, it is roughly 93%. Because there is a distribution of bubble sizes at any given time in the life of the foam, the bubbles can pack to fill 93% of space while still remaining relatively spherical. Nevertheless, even if the bubbles are in a relaxed state in their initial spatial arrangements, as they coarsen, their spatial orientation will no longer be ideal to fill the required amount of space. This will cause the bubbles to become distorted in shape, costing elastic energy and inducing stresses due to their surface tension. Eventually, the stresses will cause the bubbles to rearrange themselves, adopting new positions to reduce the stresses. These rearrangement events are clearly visible by observing the foam in a microscope, although multiple scattering restricts the observation of these events to those occurring near the surface. It is these rearrangement events that lead to the decay of the autocorrelation function observed with DWS.

In Foamy, the bubbles are sufficiently stabilized by surfactant that coarsening is restricted to the Ostwald ripening mechanism. This occurs relatively slowly, and the foam retains its characteristics for a considerable length of time. However, after it is first produced, DWS measurements in both the backscattering and transmission geometries exhibit correlation functions that have the same form as those observed with diffusing particles, despite the fact that there are no particles undergoing diffusive motion in the foam which could result in this sort of decay. Instead, the only dynamics that can be observed by microscopic observation of the surface of the foam are the rearrangement events. Thus, we must develop a new model for DWS to account for the effects of these rearrangements on the autocorrelation function.

We again assume that the diffusion approximation describes the transport of the light through the medium. Then, we calculate the decay of the autocorrelation function for each diffusive light path due to the rearrangement events. Since the experiment shows that the paths decay in the same fashion as those measured for diffusing particles, we expect the autocorrelation functions for the individual paths to decay exponentially, with the exponent exhibiting a linear dependence on both the path length and time. This

will ensure that the Laplace equation for the total autocorrelation function, eq. (6), again results in the functional forms that are measured.

When it is first sprayed from the can, the typical bubble size in Foamy is about $20\ \mu\text{m}$ in diameter, and therefore is much larger than the wavelength of light. When the bubbles undergo a rearrangement event, their motion is over length scales that are comparable to their sizes, and hence much greater than the wavelength. As a result, any light paths that pass through the volume affected by the rearrangement event will be changed in length by an amount much greater than a wavelength. This will totally randomize the phase of these paths and therefore result in the decay of their contribution to the autocorrelation function. The contribution to the autocorrelation function from all the paths of length s will decay completely when rearrangement events have occurred in all the paths. Furthermore, the probability of decay of the unrandomized paths will be proportional to the number remaining, so that the decay will grow exponentially in time. The decay rate will also be proportional to the likelihood that the path will intercept a rearrangement event. This probability increases with the volume of the path, which is determined by the product of its length and its cross-sectional area. The length of the path is s , while its cross-sectional area is l^{*2} , since this length scale determines the diffusive light path. We assume that the rearrangement events occur with a probability of R events per unit volume per unit time. In addition, we introduce an efficiency factor that accounts for the effectiveness of any rearrangement event in causing a path to decay. To cause the phase of a path to be totally randomized, the rearrangements must occur over a length of l^* . Thus, if we take the average length scale for rearrangement events to be r , the effectiveness of any given event will be proportional to the ratio of its volume to the volume necessary to randomize the path, $(r/l^*)^3$. The contribution of paths of length s , with n scattering events, to the total decay of the autocorrelation function is then

$$g_1^n(t) = e^{-Rr^3(s/l^*)t}. \quad (22)$$

This has the form required to lead to the experimentally observed results: it is linear in both s and t , and thus when used in the Laplace equation, eq. (6), it will yield autocorrelation functions with the same functional form as those observed for diffusing particles. The same solutions, eqs (7), (8) and (9) will hold for foams, with the substitution of Rr^3 for $1/\tau_0$. Thus DWS probes the rate of occurrence of a rearrangement event in any given volume of the foam.

This prediction can be tested for Foamy by comparing the rate of rearrangement events measured with DWS with that extrapolated for the bulk of the foam from observation of the rate of rearrangements at the surface observed with a microscope. For Foamy, the rate of these rearrangements decreases markedly with time, so that following the behavior of the foam as it ages allows a critical test of this theory for DWS from foams. Excellent correlation is found between the DWS results and those measured microscopically [34], verifying the validity of this expression, eq. (22). This correlation extends over three orders of magnitude in R . Thus, DWS provides a new method for studying the dynamics of foams, and determining the characteristic time scales of the rearrangements of the bubbles. This might be particularly

useful as a method for studying the microscopic basis for the fascinating rheology of foams. Their rheology must be dominated by the motion of the bubbles with respect to one another, and it is this motion to which DWS is directly sensitive. More generally, these results illustrate the utility of DWS for the study of dynamic events that are both temporally and spatially rare.

4. Conclusions

We have discussed the extension of dynamic light scattering techniques to very strongly scattering media, where multiple scattering of the light is so significant that light propagation through the media is well described by the diffusion approximation. In this limit, it is possible to quantitatively analyze the autocorrelation functions. This is accomplished by using the diffusion approximation to determine the distribution of paths followed by the photons propagating through the medium, and to determine the length and number of scattering events for each path. We assume that each path contributes independently to the total autocorrelation function as all the interference occurs only at the detector, outside of the sample, and not within the sample. To calculate the autocorrelation function of each path, we assume that it is comprised of a sufficiently large number of scattering events that we can neglect the detailed conservation of momentum for each scattering event. Instead, we replace the contribution of each scattering event by an average that reflects the distribution determined by the form factor of the scatterers. Then, if each scattering event is independent, the autocorrelation function of a path of n scattering events is the product of n contributions of the average. The total autocorrelation function is the sum of the contributions from the individual paths, weighted by the probability that a photon follows that path. By this procedure, we are able to quantitatively calculate the functional form of the correlation function and relate its decay to the dynamics of the scattering medium.

Because the light is multiply scattered, the scattering angle and wave vector do not possess the same significance that they do in a single scattering experiment. In fact, since the contribution from each scattering event is replaced by an angular average, the autocorrelation function of a single path has already accounted for the average over all scattering angles. Thus, the final angle of detection of the light is not critical. Instead, the autocorrelation function depends on the geometry of the experiment. One useful geometry is that of transmission, where the sample is illuminated on one side and the light that has propagated through the sample to the other side is collected and analyzed. We present two functional forms for transmission. The first is for the case where the incident beam is focused to a point, and the light is collected from a point on the other side of the sample, on axis with the incident beam. The second case accounts for the results obtained when the incident beam is expanded to fill the whole sample face, while the transmitted light is still collected from a point on the other side of the sample. Different results are obtained if the scattered light is collected from a point on the same side of sample that is illuminated by an expanded beam, in the backscattering geometry.

We have also illustrated the usefulness of DWS by exploring some examples of the dynamics that can be probed. Our emphasis has been on the novel dynamics that are accessible

through the use of DWS, and cannot be studied by traditional dynamic light scattering techniques. Since DWS probes multiply scattered light, the decay of the autocorrelation function reflects the change in length of a diffusive light path. This decay results from the aggregate motion of a large number of particles that contribute to the scattering path. Thus, while the total path length must change by a full wavelength, the motion of each individual scatterer can be substantially less. Therefore, DWS can probe motion on very short length scales. Here, we exploit this feature to study the time evolution of hydrodynamic interactions between particles in concentrated suspensions of hard spheres.

We are able to probe the motion of the scattering particles on sufficiently short length scales that we can determine the decay of their velocity correlation function. We show that it does not decay exponentially, but rather its decay is algebraic, with $t^{-3/2}$ time dependence. This behavior was first predicted from computer simulations, and is known as the "long-time" tail of the velocity correlation function. As a result, the time-dependent self-diffusion coefficient of the particles approaches its asymptotic value only very slowly. We also study the dependence of the time-dependent self-diffusion coefficient on the volume fraction of spheres. We find that velocity correlation function has the same $t^{-3/2}$ decay for all volume fractions. Moreover, we show that time-dependent self-diffusion coefficients for all volume fractions can be scaled onto a single curve, whose functional form can be determined theoretically by the behavior of a single sphere interacting with the surrounding fluid. The scaling parameters for the horizontal and vertical directions have markedly different dependencies on volume fraction. The scaling parameter for the vertical direction reflects the asymptotic value of the self-diffusion coefficient at time scales longer than the decay of the velocity correlation function, but shorter than the time scales for relaxation of the particle positions. The measured ϕ -dependence of this scaling parameter is consistent with tracer measurements performed with single scattering DLS. By contrast, the scaling parameter for the horizontal direction represents a new viscous time scale. Its measured ϕ dependence is described by the behavior of the inverse of the high-frequency, low-strain viscosity of the suspension. This suggests that the behavior of the hydrodynamic interactions can be described by an effective medium approach: as the vorticity diffuses away from a particle, it no longer distinguishes the presence of individual spheres, but instead is sensitive only to the medium comprised of the suspension of particles in the fluid. Surprisingly, however, the observed scaling behavior persists to very short times, implying that the fluid flow is determined by the full suspension at much shorter times than expected.

We also present measurements of the behavior of very small spheres, where the light scattering is sensitive to both the self diffusion coefficient as well as the effects of the relative motion of neighboring particles. We again find that the data can be scaled onto a single curve. However, the time scales determined from the scaling are significantly shorter than for the same volume fraction of the larger spheres. By contrast, measurements of the behavior of these particles at even shorter times indicate that the scaling times are similar to those measured with larger particles. This implies that the

time evolution of the hydrodynamic interactions between neighboring particles has a markedly different behavior than that observed for the interactions of the particle itself with the surrounding suspension. The interparticle effects seem to begin to be effective at a somewhat later time.

Finally, we have also presented a brief account of another useful application of DWS. This application exploits the very large volume probed by the diffusion of the light within the sample. It facilitates the study of dynamics that are both temporally and spatially rare. We develop a new model to describe the dynamics of relatively large scale random motions in foams as they coarsen. We apply these techniques to study the behavior of a prototypic foam, shaving cream, and show how DWS can probe the rearrangement of the bubbles of air that make up the foam. This rearrangement is driven by the relaxation of the stresses incurred as the foam coarsens through a process similar to Ostwald ripening. This application of DWS provides new insight into the dynamics of a foam, that would be difficult to obtain by any other means.

Traditional dynamic light scattering techniques have proven extremely valuable in assisting our understanding of a wide range of dynamic processes. However, they have in the past been strictly restricted to nearly transparent materials, limiting the types of samples to which they could be applied. The development of diffusing wave spectroscopy alleviates this restriction, and enables the study of a wide array of new systems. This will also make it possible to investigate a wide variety of new physics problems. This paper has summarized the essential physics of the technique of DWS and has provided several examples of the new types of physics problems that can be addressed.

References

1. van Albada, M. P. and Lagendijk, A., *Phys. Rev. Lett.* **55**, 2692 (1985).
2. Wolf, P. E. and Maret, G., *Phys. Rev. Lett.* **55**, 2696 (1985).
3. Ishimaru, A., "Wave Propagation and Scattering in Random Media" (Academic, New York 1978).
4. Wolf, P. E., Maret, G., Akkermans, E. and Maynard, R., *J. Phys. France* **49**, 63 (1988).
5. Berne, B. J. and Pecora, R., "Dynamic Light Scattering: with Applications to Chemistry, Biology and Physics" (Wiley, New York 1976).
6. Pine, D. J., Weitz, D. A., Zhu, J. X. and Herbolzheimer, E., *J. Phys. France* **51**, 2101 (1990).
7. Pine, D. J., Weitz, D. A., Maret, G., Wolf, P. E., Chaikin, P. M. and Herbolzheimer, E., in "Scattering and Localization of Classical Waves in Random Media" (Edited by P. Sheng) (World Scientific, Singapore 1990).
8. Maret, G. and Wolf, P., *Z. Phys.* **B65**, 409 (1987).
9. Lagendijk, A., Vreeker, R. and DeVries, P., *Phys. Lett.* **A136**, 81 (1989).
10. Zhu, J. X., Pine, D. J. and Weitz, D. A., *Phys. Rev.* **A44**, 3948 (1991).
11. Weitz, D. A., Zhu, J. X., Durian, D. J. and Pine, D. J., in "Structure and Dynamics of Strongly Interacting Colloids and Supramolecular Aggregates in Solution" (Edited by S. H. Chen, J. S. Huang and P. Tartaglia) (Kluwer, Dordrecht 1992), p.731.
12. Weitz, D. A. and Pine, D. J., in "Dynamic Light Scattering: The Method and Some Applications" (Edited by W. Brown) (Oxford University Press, Oxford 1993), p. 652.
13. Zhu, J. X., Weitz, D. A. and Klein, R., in "Localization and Propagation of Classical Waves in Random and Periodic Structures" (Edited by C. M. Soukoulis) (Plenum, New York 1993).
14. Zhu, J. X., Pine, D. J., Chaikin, P. M., Xue, J. Z. and Weitz, D. A., to be published.
15. Pusey, P. N. and Tough, R. J. A., *Faraday Disc. Chem. Soc.* **76**, 123 (1983).

16. Fraden, S. and Maret, G., *Phys. Rev. Lett.* **65**, 512 (1990).
17. Qiu, X., Wu, X. L., Xue, J. Z., Pine, D. J., Weitz, D. A. and Chaikin, P. M., *Phys. Rev. Lett.* **65**, 516 (1990).
18. Zhu, J. X., Durian, D. J., Muller, J., Weitz, D. A. and Pine D. J., *Phys. Rev. Lett.* **68**, 2559 (1992).
19. Burstyn, H. C. and Sengers, J. V., *Phys. Rev.* **A27**, 1071 (1983).
20. Pine, D. J., Weitz, D. A., Chaikin, P. M. and Herbolzheimer, E., *Phys. Rev. Lett.* **60**, 1134 (1988).
21. Weitz, D. A., Pine, D. J., Pusey, P. N. and Tough, R. J. A., *Phys. Rev. Lett.* **63**, 1747 (1989).
22. Hinch, E. J., *J. Fluid Mech.* **72**, 499 (1975).
23. Alder, B. J. and Wainwright, T. E., *Phys. Rev. Lett.* **18**, 988 (1967).
24. Paul, G. L. and Pusey, P. N., *J. Phys. A.* **14**, 3301 (1981).
25. Beenakker, C. W. J. and Mazur, P., *Phys. Lett.* **A98**, 22 (1983).
26. Beenakker, C. W. J. and Mazur, P., *Physica* **126A**, 349 (1984).
27. van Veluwen, A., Lekkerkerker, H. N. W., de Kruijff, G. C. and Vrij, A., *Faraday Discuss. Chem. Soc.* **83**, 59 (1987).
28. van Megan, W., Underwood, S. M., Ottewill, R. H., Williams, N. S. J. and Pusey, P. N., *Faraday Discuss. Chem. Soc.* **83**, 47 (1987).
29. Beenakker, C. W. J., *Physica* **128A**, 48 (1984).
30. Ladd, A. J. C., *Phys. Rev. Lett.* **70**, 1339 (1993).
31. Percus, J. K. and Yevick, G. J., *Phys. Rev.* **110**, 1 (1958).
32. Kao, M. H., Yohd, A. G. and Pine, D. J., *Phys. Rev. Lett.* **70**, 242 (1993).
33. Durian, D. J., Weitz, D. A. and Pine, D. J., *Science* **252**, 686 (1991).
34. Durian, D. J., Weitz, D. A. and Pine, D. J., *Phys. Rev.* **A44**, R7092 (1991).